Original Article

A mechanobiological approach to find the optimal thickness for the locking compression plate: Finite element investigations

Yousof Mohandes[1] [iD], Masoud Tahani[1], Gholamreza Rouhi[2] [iD] and Mohammad Tahami[3]

Abstract

This study aimed at finding the acceptable range, and the optimal value for the locking compression plate (LCP) thickness (THK), through simulating the osteogenic pathway of bone healing, and by checking bone-plate construct's strength and stability. To attain the goals of this research, a multi-objective approach was adopted, which should trade-off between some conflicting objectives. A finite element model of the long bone-plate construct was made first, and validated against an experimental study. The validated model was then employed to determine the initial strength and stability of the bone-plate construct, for the time right after surgery, for various thicknesses of the LCP. Afterward, coupling with a mechano-regulatory algorithm, the iterative process of bone healing was simulated, and follow up was made for each LCP thickness, over the first 16 post-operative weeks. Results of this study regarding the sequence of tissue evolution inside the fracture gap, showed a similar trend with the existing in-vivo data. For the material and structural properties assigned to the bone-plate construct, in this study, an optimal thickness for the LCP was found to be 4.7 mm, which provides an enduring fixation through secondary healing, whereas for an LCP with a smaller or greater thickness, either bone-implant failure, unstable fixation, impaired fracture consolidation, or primary healing may occur. This result is in agreement with a recent study, that has employed a comprehensive optimization approach to find the optimal thickness.

Introduction

Diaphyseal bone fracture is a common orthopedic problem, which may stem from deteriorative effects of aging or other comorbidities, lack of enough nutrition, genetic disorders, traumatic injuries, or progressive damage accumulation.[1–3] To mechanically stabilize and anatomically align the mobile fragments of a broken bone, a functional reduction and a stable fixation must be employed.[4] Among the common reconstruction hardware, bone plates are frequently used to restore the function and mobility of the injured limb back to its original form and quality.[5,6] However, in spite of their widespread usage, there are some side effects attributed to them. The serious clinical complications in plate fixations are secondary fracture of bone, failure of the implant, and non-union or mal-union of bone.[7] Mechanical factors contribute significantly in escalating or lessening the postoperative complications.[8] Construct failure may either come from insufficient strength of bone and implant, or due to high applied loads. Non-union ensues from inadequate stability of the fixation. Mal-union is chiefly manifested due to stiffness mismatch between bone and surgically

[1]Department of Mechanical Engineering, Ferdowsi University of Mashhad, Mashhad, Iran
[2]Department of Biomedical Engineering, Amirkabir University of Technology, Tehran, Iran
[3]Bone and Joint Research Center, Shiraz University of Medical Sciences, Shiraz, Iran

Corresponding author:
Masoud Tahani, Faculty of Engineering, Department of Mechanical Engineering, Ferdowsi University of Mashhad, Azadi Square, Mashhad, Razavi Khorasan Province 91775-1111, Iran.
Email: mtahani@um.ac.ir

implanted plate.[9] Indeed, in a bone-plate assembly, although the metallic implant is suitable to provide a mechanically strong and stable condition, but since metals are much stiffer than bone, there is a tendency for metallic plate to sustain a considerable part of the applied load on the bone-plate construct. Hence, the flow of stress in a fixed long bone is deviated from its normal way and it bypasses the fracture site by transmitting through the bridging plate.[9] Owing to this reason, progenitor stem cells in callus are deprived of sensing sufficient mechanical signals which are vital for desirable healing in patients.[10]

To investigate how mechanical milieu regulates dynamic processes of bone healing, mechanobiology of bone healing must be cited. Accordingly, repair of a long bone is classified into two classic pathways: primary and secondary healing.[11] In case of absolute fixation, imposed by rigid implants, direct bone formation via osteogenic pathway occurs, which is known as primary or direct bone healing process. In the other scenario, when a less rigid fixation technique is implemented, secondary or indirect bone healing is expected to happen and proceed along chondrogenic pathway.[12] So far, several theories have been developed, to address the implications of mechanical factors on the outcomes of bone healing.[11,13–18]

To achieve a desirable fixation, which results in an optimal bone healing process, without compromising the strength and stability of the construct, it is imperative to either optimize currently used, or introduce new generation of plates. Even though elastic modulus of bone plate has attracted the attention of many researchers to attain and maintain more balanced load carrying capacity between bone and plate,[19–23] but tracing the healing course and tissue differentiation upon alteration in plate stiffness through its thickness has not been reflected in the currently available literature. Comprehensively, different basic criteria, including bone healing process, strength and stability of the bone-plate construct, should be simultaneously involved in order to find out an optimal plate thickness which results in a most successful healing. In healing process of a long bone, a plate which provides continual and gradual consolidation process of healing and produces intermediate soft medium, rather than immediate hard bony bridge, at early stages of healing, can be of interest.[24] Nonetheless, the construct should be strong enough to resist the applied load, particularly at the initial phase after surgery, when the fracture gap is completely filled with a soft granulation tissue. Moreover, an advisable plate should be stiff and stable enough to impede unnecessary extra-motions inside the fracture site, in order to avoid excessive deformation of granulation tissue at early stages of healing and deliver the maximum amount of mature bone at the end of the healing process. Otherwise, there will be soft tissue production, or premature bone tissue formation, which can be deemed as either mal-union or non-union of the healing process.[6]

In this work, to find the optimal thickness of the 8-hole LCP, a multi-objective design method, along with in-silico simulations was employed, in which the effects of the thickness, on the overall strength and stability of the construct, as well as on the evolution of healing pattern, were investigated. Deviatoric strain theory, was employed as the mechano-regulation algorithm for bone healing, which suggests that deviatoric component of strain tensor is a determinant factor in guiding the tissue differentiation in callus during bone healing.[18]

Materials and methods

The commercial finite element software, Abaqus (V 6.14-1, Simulia, Dassault Systems) was used to create geometries, assign material properties, and to define load and boundary conditions of the bone-plate compound. The FE model was composed of a lower extremity long bone, a simplified model of tibia,[25] with a simple transverse fracture, and a straight LCP that bridges the fracture gap with locking screws, shown in Figure 1(a) and (b). The mid-shaft of an adult tibia was simplified as a 300 mm long cylinder, with the outer and inner diameters of 25 and 15 mm,[26] respectively, which its intermedullary canal was filled with bone marrow, Figure 1(c). A fracture gap of 3 mm was considered in the middle of the bone model to mimic midshaft fracture.[27] The central part of healing tissue was modeled as a disc with a 3 mm thickness and a 25 mm diameter, filling the fracture gap, while the external part was modeled as an oval which extends 30 mm along the periosteum.[18] Callus index, which was defined as the ratio of oval diameter at the fracture site to the outer bone diameter, was set to be 1.1,[27] Figure 1(c). An 8-hole LCP with a length of 152 mm and width of 13.5 mm, was fixed at a 1 mm distance above the periosteum,[28] by means of six locking head, bi-cortical screws positioned at 123,678 configuration,[29] while two holes close to the fracture site were kept empty, Figure 1 (b) and (c). Diameter of screws was 4.5 mm and their length, depending on LCP thickness, was changed between 28 to 34 mm. The FE model was regenerated seven times, each corresponds to a certain LCP thickness, which was the independent variable in this study. LCP thicknesses of: 2, 3, 4, 5, 6, 7, and 8 mm were examined here, which comprised the range of frequently used thicknesses for bone plates. To simulate the locking feature of the construct, the contact surfaces between plate and screws were assumed to be tied together. Moreover, adjacent nodes at the interfaces of screws and cortical bone were also assumed to be tied together.

All degrees of freedom, at the bottom distal end, were constrained throughout the simulation, and the axial compressive load was uniformly distributed at the top proximal end of the bone model, throughout healing simulation, Figure 1 (a). To account for the gradually increasing weight bearing capacity of fixed bone
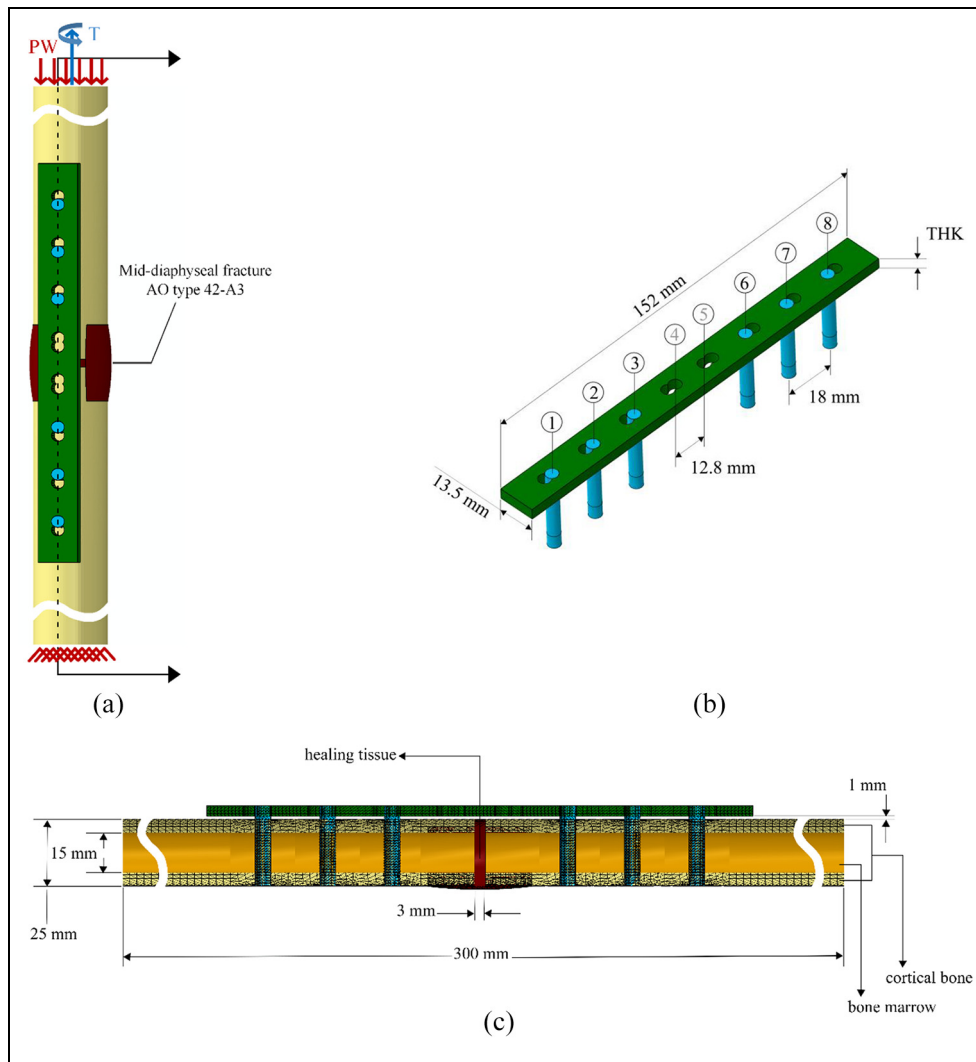
Figure 1. (a) Schematic depiction of bone-plate-screw assembly, used in the FE model, applied loads and boundary condition, (b) an 8-hole LCP fixed by six locking head screws in 123,678 configuration, and (c) a section view of the construct illustrating how the fixation was achieved.

during post-operative rehabilitation process, a controlled amount of partial patient's weight (PW) with a total body weight of 75 kg were assumed to be applied progressively in a sequential order. According to the post-operative management guideline suggested by AO foundation,[30] an initial partial weight equals to 25% of body weight, was increased to 50% for the periods between weeks 6 and 10, then was promoted to full body weight for the rest of healing. For evaluating the initial strength and stability of the construct, besides an axial compressive load case equal to 25% of body weight, another load case, in the form of pure torsional moment (T), equals to 7 N.m., was considered,[31] Figure 1(a).

For bone, LCP, as well as all locking screws, isotropic, linear elastic properties were considered.[32] Properties for all materials are presented in Table 1.

Callus elements were assumed with variable modulus of elasticities for subsequent steps of bone healing process, which were modulated by local mechanical stimulus inside each element. Based on the mechano-

Table 1. Material properties used for cortical bone, bone marrow, LCP and screw in the FEA of this study.[18,32–34].

Material	Young's modulus (GPa)	Poisson's ratio	Allowable stress (MPa)
Cortical bone	20	0.3	111
Bone marrow	0.002	0.167	–
LCP and screw	200	0.3	690

regulation algorithm of bone healing used in this study,[18] deviatoric strain (ε_d), equation (1), is the mechanical stimulus in each element:

$$\varepsilon_d = \frac{2}{3} \sqrt{(\varepsilon_1 - \varepsilon_2)^2 + (\varepsilon_1 - \varepsilon_3)^2 + (\varepsilon_2 - \varepsilon_3)^2} \qquad (1)$$

where $\varepsilon_1, \varepsilon_2$ and ε_3 are principal strains in each element. In Table 2, material properties and expected tissue

Table 2. Properties and tissue phenotypes of callus elements in term of deviatoric strain.[18].

Deviatoric strain (ε_d)	Tissue type	Young's modulus (MPa)	Poisson's ratio
$\varepsilon_d = 1$	Granulation tissue	1	0.167
$0.05 \leqslant \varepsilon_d < 1$	Fibrous	1–5	0.167
$0.025 \leqslant \varepsilon_d < 0.05$	Cartilage	5–500	0.167
$0.0005 \leqslant \varepsilon_d < 0.025$	Immature bone	500–1000	0.325
$0.00041 \leqslant \varepsilon_d < 0.0005$	Intermediate bone	1000–2000	0.325
$0.00005 \leqslant \varepsilon_d < 0.00041$	Mature bone	2000–6000	0.325
$\varepsilon_d < 0.00005$	Resorption	-	-

Table 3. Number of elements for LCPs and screws, based on the plate thickness.

|	LCP Thickness (mm)						
	2	3	4	5	6	7	8
Number of elements for LCP	28,201	39,759	52,202	62,539	74,610	85,025	96,280
Number of elements for each screw	3062	3185	3302	3379	3520	3785	3897

phenotypes of callus elements are expressed as a function of deviatoric strain.[18]

Three dimensional quadratic solid elements (C3D10) were used to discretize the bone, healing tissue, plate, and screw domains into tetrahedral pieces. Mesh refinement study was performed until the difference in the pattern of tissue differentiation, and the total axial displacement of the construct between two subsequent analyses were within 2%. Accordingly, the size of elements in in healing tissue, plate, and screw were stabilized at the global size of 1 mm. For bone segments, global element size was converged at 2 mm, except at the edges and surfaces of the bone-holes which were in direct contact with screws, and thus were seeded with 1 mm elements, locally. Bone and healing tissue were meshed with 173,554 and 24,084 elements, respectively. Table 3 shows the number of elements generated in LCPs and screws, based on plate thicknesses.

The finite element model utilized in this study was validated against the results of an experiment which had been carried out to evaluate the axial stiffness of a fractured bone fixed by an LCP and locking screws.[35] The experimental construct was composed of a composite humerus with a mid-shaft gap of 10 mm between its two fragments, fixed by an 8-hole 3.5 mm LCP.[35] An FE model of that experimental construct was created in this work to simulate the axial compression test.

In this study, as the work flowchart of Figure 2 shows, FE simulations were conducted three times for each thickness of the LCP, to assess its performance. First and second simulations were associated with measuring the initial strength and stability of the construct, at the beginning of healing, under axial compressive load, also due to a pure torsional moment. The third simulation was made on the healing processes over the period of 16 post-operative weeks.

For the stress analysis of different parts of the construct with regard to their relevant yield strength,
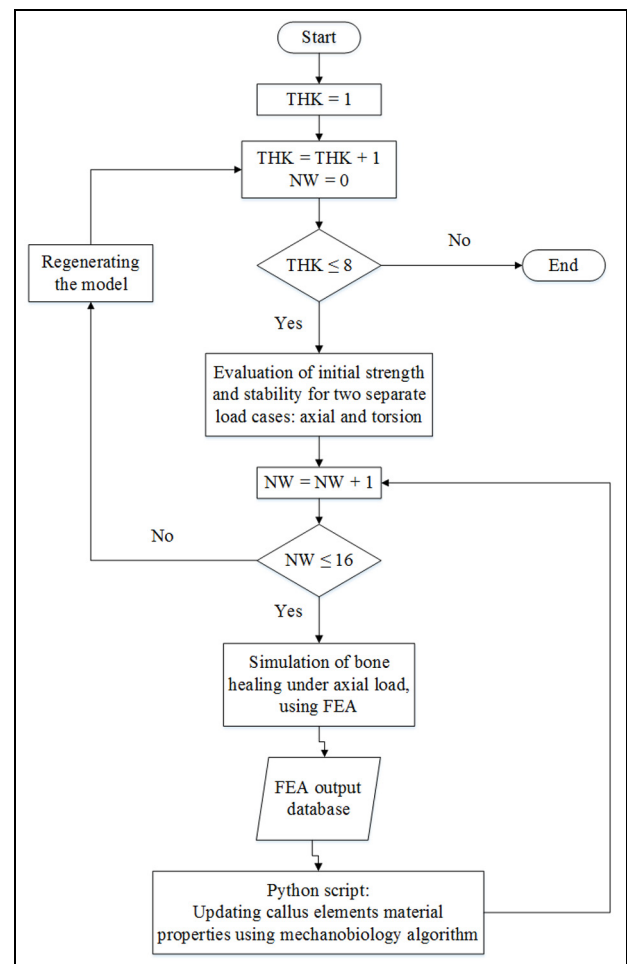
Figure 2. Flowchart of iterative computational procedure used in this study. THK and NW stand for the thickness of LCP and the number of weeks after surgery, respectively.

maximum von Mises stresses resulted in bone, LCP, and screws were determined. To evaluate the initial stability of the construct, interfragmentary axial strain
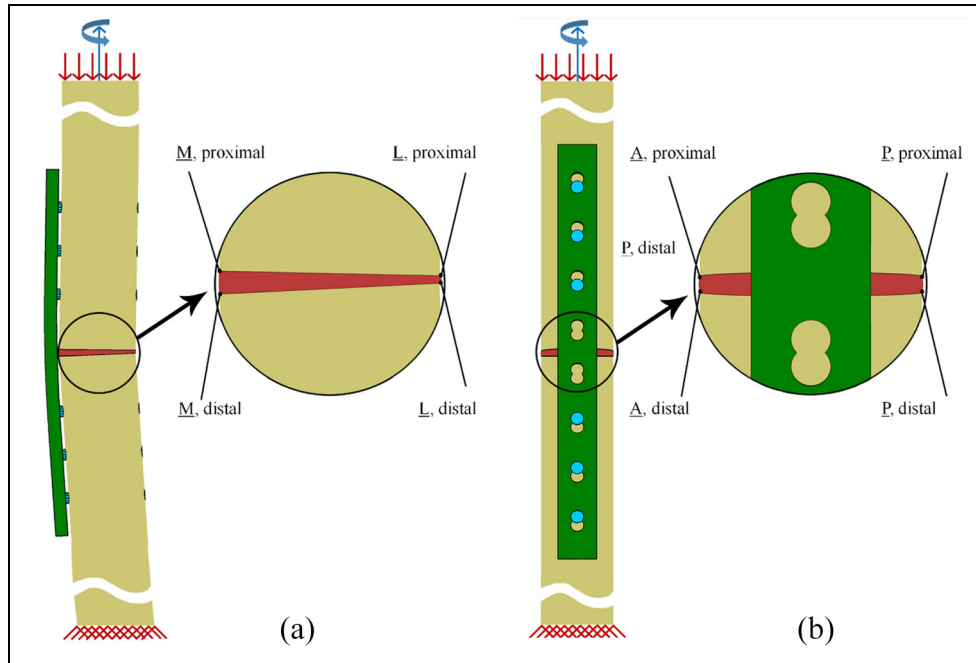
Figure 3. Positions of nodes were used to calculate IFAS and IFSM: (a) nodes located on the periosteum borders of distal and proximal segments of bone, adjacent to fracture site at medial (M) and lateral (L), and (b) anterior (A) and Posterior (P) sites. External callus was not shown in this figure, for better illustration of nodes.

(*IFAS*) and interfragmentary shear movement (*IFSM*) of initial granulation tissue at the fracture site, were calculated, under axial load and torsion moment, respectively. To calculate *IFAS*, relative axial displacements (Δ_A) of adjacent nodes located on the distal and proximal segments of cortical bone were determined at medial ($\underline{M}$), lateral ($\underline{L}$), anterior ($\underline{A}$), and posterior ($\underline{P}$) positions on the periosteum of bone segments, near the fracture site, as shown in Figure 3(a) and (b), using equation (2):

$$\Delta_{A\underline{i}} = \Delta_{A\underline{i}, proximal} - \Delta_{A\underline{i}, distal} \quad i = \underline{M}, \underline{L}, \underline{A}, \underline{P} \tag{2}$$

Then the maximum value of relative axial displacements was divided by the fracture gap length (l), using equation (3):

$$IFAS = Max(\Delta_{A\underline{M}}, \ \Delta_{A\underline{L}}, \ \Delta_{A\underline{A}}, \ \Delta_{A\underline{P}})/l \tag{3}$$

To determine *IFSM*, relative tangential displacements (Δ_T), were calculated using equation (4):

$$\Delta_{Tj} = \Delta_{Tj, proximal} - \Delta_{Tj, distal} \quad j = \underline{M}, \underline{L}, \underline{A}, \underline{P} \tag{4}$$

Then, the maximum of relative tangential displacements was introduced as *IFSM*, using equation (5):

$$IFSM = Max(\Delta_{T\underline{M}}, \ \Delta_{T\underline{L}}, \ \Delta_{T\underline{A}}, \ \Delta_{T\underline{P}}) \tag{5}$$

The *IFAS* and *IFSM* were checked with their maximum allowable values, that is, 33% and 1.5 mm, respectively, which were considered as deleterious upper thresholds for the normal healing process.[36,37] Beyond these limits, *IFAS* and *IFSM* were assumed to cause damages to granulation tissue and the condition were defined as unstable, throughout this study.

To computationally investigate the evolution of ossification sequences for a time period of 16 weeks after surgery, a user defined Python script was written based on an algorithm for a mechanobiological model of bone healing process.[18] Progenitor stem cells, originated from periosteum layer, central callus-cortical bone interface and bone marrow, were assumed to migrate to fracture site, by the diffusion equation[38]:

$$D\nabla^2 n = \frac{dn}{dt} \tag{6}$$

where n is the cell concentration, t represents number of week after surgery and D is a constant diffusion coefficient. Each healing simulation was carried out for 16 iterations and D was found so that all callus elements reach full cell concentration by the end of 16th iteration.[38] In this regard, each iteration was equivalent to 1 week of the healing process. In the first iteration, the callus was filled with granulation tissue, and at the end of the iteration, cell concentration and strain field output for each callus element were determined and transferred from Abaqus output database into a user defined script. The average value of deviatoric strain was then calculated for each element within the callus, in order to recognize new tissue composition according to the employed mechano-regulatory algorithm,[18] Table 2. To account for gradual evolution of tissue type, a rule of
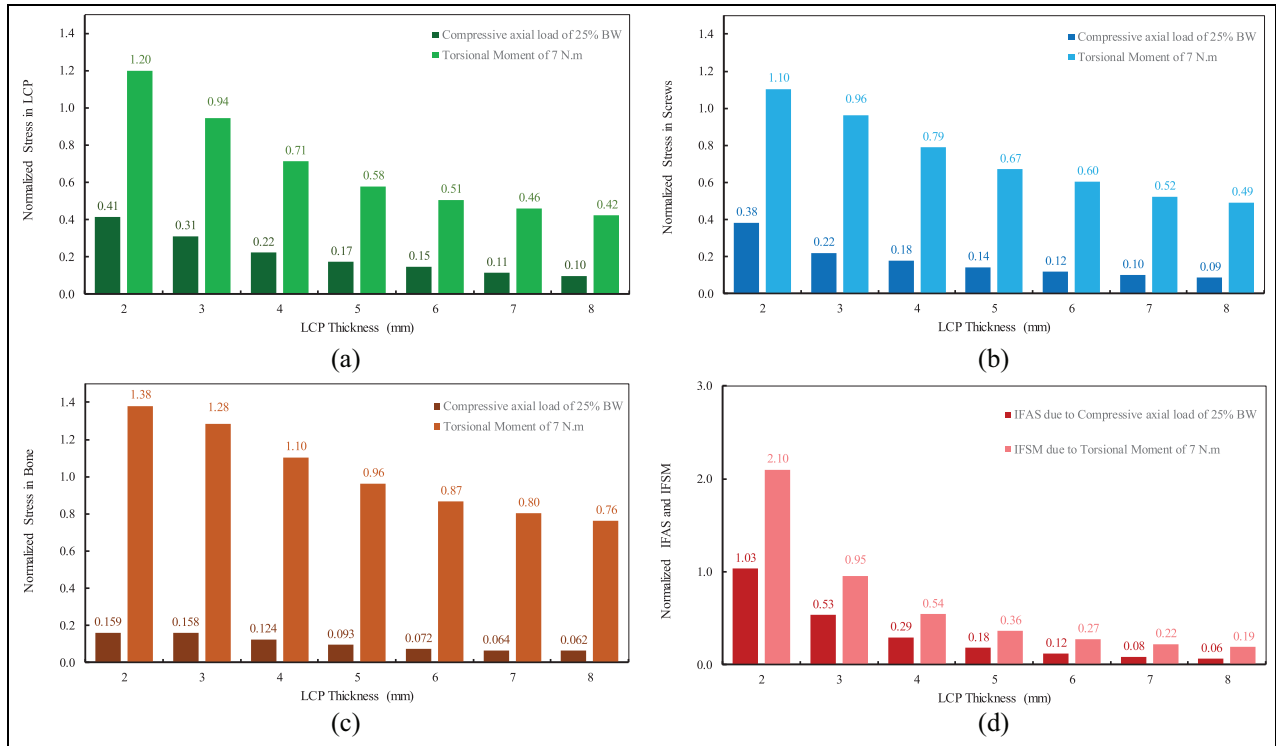
Figure 4. Normalized maximum von Mises stress in: (a) LCP, (b) screws, (c) bone, under axial compressive load, and torsional moment, and normalized (d) IFAS, and IFSM at the callus, immediately after surgery, when plate thickness changes from 2 to 8 mm. BW is an abbreviation for the body weight.

mixture[32] were used to obtain new modulus of elasticity of each element. Then, material properties of each callus element were updated, and new iteration began with new material properties assigned to callus elements, and this procedure was repeated up to 16th iteration.

Results

The axial stiffness of an FE model, which simulated an experimental study,[35] was 473 N/mm, similar to the axial stiffness resulted from the mechanical experiment, that is 475.6 ± 63 N/mm.

Results of stress analysis for plate, bone and screws under two different loading, also *IFAS*, and *IFSM* at the fracture site can be seen in Figure 4, for different thicknesses of LCP. Maximum von Mises stress for each part was normalized by dividing to its corresponding allowable stress (Table 1). *IFAS* and *IFSM* were also normalized with by dividing to their allowable thresholds, that is, 33% and 1.5 mm, respectively (Figure 4(d)). Values reported in Figure 4(a) to (d) are associated with the outcomes of the first and second finite element analyses for each LCP, immediately after surgery and prior to the ossification of granulation tissue, when the fracture site had the least mechanical integrity and strength.

Time-dependent distribution of six distinct tissue types, as well as resorption over the callus domain, versus thickness of the 8-hole LCP, during the 8 weeks after surgery, can be found in colorful contours of Figure 5(a), accompanied with a color legend (Figure 5(b)).

The percentage of granulation, which is within the central and external callus and, converted into fibrous and/or cartilage tissue at the end of the first week after surgery, for various plate thicknesses can be seen in Table 4. The total amount of fibrous and cartilage tissues, reflects the tendency of stem cells to pass through secondary bone healing process, which can be seen in regions with light, medium and dark blue colors in Figure 5(a).

Table 5 shows the percentage of callus elements converted to premature bone, fibrous and cartilage tissue, predicted at the end of 16 weeks after surgery, when the plate thickness changes from 2 to 8 mm.

A summary on the performance of the 8-hole LCP, with different thicknesses, employing various criteria, that is, inclination for secondary healing, fracture union, initial bone-LCP-screw strength, and initial stability of bone-LCP-screw construct, can be seen in Table 6. Acceptable range of plate thickness could be obtained versus each criterion, depend on the material and structural properties of the whole construct, which were considered in this study, as illustrated in Figure 1 and Table 1.

Discussion

In this work, the effects of the locking compression plate thickness on the major aspects of a successful
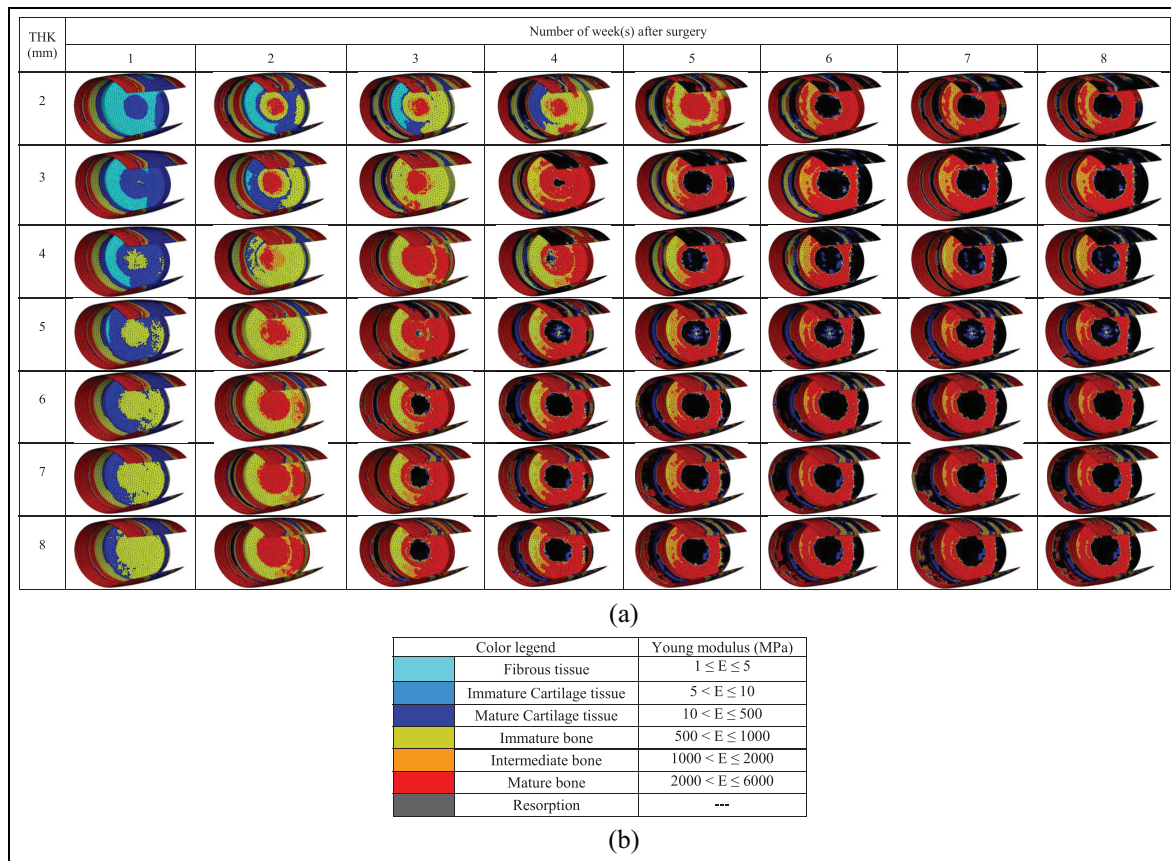
(a)

Color legend		Young modulus (MPa)
	Fibrous tissue	$1 \leq E \leq 5$
	Immature Cartilage tissue	$5 < E \leq 10$
	Mature Cartilage tissue	$10 < E \leq 500$
	Immature bone	$500 < E \leq 1000$
	Intermediate bone	$1000 < E \leq 2000$
	Mature bone	$2000 < E \leq 6000$
	Resorption	---

(b)

Figure 5. (a) Post-operative mapping of tissue distribution within the callus, for various thicknesses ($2 \leqslant THK \leqslant 8$ mm) of LCP for first 8 weeks after surgery and (b) color legend for tissue mapping.

Table 4. Percentage of central callus (CC) and external callus (EC) elements converted to fibrous and/or cartilage tissue at the end of the first week after surgery, when the plate thickness was changed from 2 to 8 mm.

LCP thickness (mm)	Tissue type					
		Fibrous (%)	Immature cartilage (%)	Mature cartilage (%)	Total (%)	Total $_{CC, EC}$ (%)
2	CC	79.81	0.51	19.68	100.00	74.12
	EC	20.11	0.22	27.76	48.08	
3	CC	55.87	0.65	43.05	99.57	72.01
	EC	12.71	0.25	31.33	44.29	
4	CC	34.08	0.76	61.39	96.22	68.66
	EC	5.36	0.42	35.14	40.92	
5	CC	7.87	1.23	82.98	92.08	64.93
	EC	0.52	0.22	36.88	37.62	
6	CC	0.00	0.00	88.00	88.00	61.47
	EC	0.00	0.00	34.78	34.78	
7	CC	0.00	0.00	84.24	84.24	60.79
	EC	0.00	0.00	35.44	35.44	
8	CC	0.00	0.00	79.89	79.89	55.37
	EC	0.00	0.00	30.70	30.70	

bone reconstitution, were investigated. The main goal of this study was the optimal value of the LCP thickness, which can guarantee a durable fixation through secondary bone healing process. To this end, a finite element model, along with a user defined Python script, based on a mechano-regulatory model of a bone healing process,[18] was developed.

The results corresponding to the axial stiffness of the FE model, obtained in the validation phase of this study, showed that from mechanical point of view, the methodology used here to create the finite element model of the bone- LCP-locking screw construct is able to reproduce the results of an in-vitro experiment.[35] The results of stress analysis showed that, for axial and

Table 5. Percentage of callus elements converted to immature and intermediate bone (total premature bone), fibrous and cartilaginous tissues (total soft tissue), at the end of 16 weeks after surgery, for different thicknesses of LCP (from 2 to 8 mm).

Tissue type	LCP thickness (mm)						
	2	3	4	5	6	7	8
Immature bone (%)	12.17	9.75	8.31	6.46	5.79	5.77	5.47
Intermediate bone (%)	7.10	6.68	6.88	8.49	7.97	7.78	7.57
Total premature bone (%)	19.27	16.43	15.19	14.95	13.76	13.55	13.04
Fibrous (%)	0	0	0	0	0	0	0
Immature cartilage (%)	0	0	0	0	0	0	0
Mature cartilage (%)	1.31	1.29	0	0	0	0	0
Total soft tissue (%)	1.31	1.29	0	0	0	0	0

Table 6. Evaluation of the LCP with different thicknesses versus different design criteria (for the construct depicted in Figure 1, with the material properties reported in Table 1).

Design criteria	LCP thickness (mm)						
	2	3	4	5	6	7	8
Secondary pathway at initial stage of healing	✓	✓	✓	✓	✓	✓	✓
Absence of soft tissue at week 16	✗	✗	✓	✓	✓	✓	✓
Initial LCP strength, axial load case	✓	✓	✓	✓	✓	✓	✓
Initial LCP strength, torsional load case	✗	✓	✓	✓	✓	✓	✓
Initial screw strength, axial load case	✓	✓	✓	✓	✓	✓	✓
Initial screw strength, torsional load case	✗	✓	✓	✓	✓	✓	✓
Initial bone strength, axial load case	✓	✓	✓	✓	✓	✓	✓
Initial bone strength, torsional load case	✗	✗	✗	✓	✓	✓	✓
Initial axial stability, *IFAS*	✗	✓	✓	✓	✓	✓	✓
Initial torsional stability, *IFSM*	✗	✓	✓	✓	✓	✓	✓

Symbols ✓ and ✗ indicate approved and rejected, respectively.

torsional loading conditions, LCPs with greater thicknesses produce lower stresses in plate, screws and bone. Under axial load of 25% of body weight, at the initial stage of healing, the normalized values of maximum von Mises stress induced in LCP, screws and bone segments, were found to be lower than the unity, regardless of the plate thickness (Figure 4(a)–(c)). On the contrary, Figure 4(a) and (b) show that if bone is subjected to a torsional moment of 7 N.m. right after surgery, the LCP with a THK ⩽ 2 mm results in normalized stresses of 1.2 and 1.1 in LCP and screws, respectively. Moreover, for the torsional moment of 7 N.m., normalized bone stresses of 1.38, 1.28, and 1.10 were found which indicate the risk of bone failure is intensified, while the bone is fixed by an LCP with a thickness of 2, 3, and 4 mm, respectively (Figure 4(c)).

Initial stability condition of a bone-implant compound should be met in order to address the probability of causing damage in callus, which can occur in the early stage of granulation tissue formation. The results of this work showed that, the *IFAS* at the fracture site for THK ⩾ 3 mm (Figure 4(d)) were below the maximum allowable *IFAS*, that is 33%.[36] Likewise, results of *IFSM* indicate that soft callus, at the early phase of generation, does not experience excessive deleterious torsional deformation beyond its allowable threshold, that is 1.5 mm,[37] if fixation is made by an LCP with a

THK ⩾ 3 mm (Figure 4(d)). Therefore, initial axial and torsional stability should not be a concern when using an LCP with a THK ⩾ 3 mm (see Table 6).

The results corresponding to tissue differentiation showed that for 2 ⩽ THK ⩽ 8 mm, sequential patterns of callus healing resemble well with the general trend of secondary bone healing process,[39] in terms of initial formation of soft callus, gradual transformation and stiffening of soft callus into hard callus, and resorption of intramedullary canal (see Figure 5(a)). Moreover, in all cases, the differentiation process was significantly accomplished within the first 8 weeks after operation, and the rate of tissue transformation was diminished afterwards. A stable state of tissue composition throughout callus after eight post-operative weeks, observed in this study, was in agreement with the results of an in-vivo histomorphometric analysis of the callus in a fractured tibia,[29] which was fixed by an 8-hole LCP with a similar screw configuration as of this study.

The results presented in Table 4 indicate that, for the thickness in the range of 2 ⩽ *THK* ⩽ 8 mm, the LCP with a smaller thickness offers a better chance for fibrocartilaginous callus formation, because a plate with a smaller thickness makes a greater deviatoric strain at the fracture site. As the thickness is directly proportional to the stiffness of the LCP, the differences

observed in the sequential pattern of tissue differentiation between LCPs with different thicknesses (see Figure 5(a) and Table 4), are in agreement with the results of some previous studies.[40,41] Moreover, for all cases, the percentage of soft tissue formed at central callus at first post-operative week is higher that of the external callus, which is due to the fact that mechanical stimuli at central part are relatively higher than those of the external part.[11]

Table 5 indicates that, 16 weeks after operation, the amount of premature bone within the callus, that is, immature and intermediate bone, is affected by the LCP thickness. As can be seen in Table 5, the 8-hole LCP with a thickness of 2 mm, compared with an 8 mm thick plate, causes a 57.18% increase in the premature bone production at the end of week 16. Additionally, the presence of soft tissues at the end of week 16, showed that plates with THK $\leqslant 3$ mm may suppress ossification, and thus will result in either delayed healing or nonunion. Findings reported in Table 5, noting that the stiffness of fixation is altered by the LCP's thickness, are in agreement with the results of some previous studies,[12,42] in which reduction of fixation stiffness was associated with the delay in bone fracture healing.

Using all design criteria employed in this study, it can be concluded that for a diaphyseal tibia fracture, placement of an 8-hole stainless steel LCP, will result in a normal healing, if its thickness lies between LLR and ULR. The lower limit of the range (LLR) is determined by considering the initial strength and stability of the construct as well as callus non-union at week 16, while the absence of soft tissue at week 1 determines the upper limit of the range (ULR). Table 6 shows that LLR is a thickness greater than 4 and less than 5 mm. On the other hand, all models of various LCP thicknesses showed some amount of fibrous-cartilage tissue at first post-surgery week, thus the ULR was not located in this range, that is, $2 \leqslant$ THK $\leqslant 8$ mm (see Table 6). Therefore, thickness of 8 mm was selected as the largest acceptable thickness in this range. Using an iterative search method[43] to find the location of LLR, it was found to be 4.7. To make a comparison between the higher and lower ends of this interval, two further FE simulations were carried out using LCPs with a thickness of 4.7 mm and 8 mm, respectively. It was found that compared with that of the 8 mm thick LCP, the LCP with a 4.7 mm thickness is less desirable, if one focuses on the fracture union criterion, since the later leads to a 7.09% more premature bone tissue formation at the end of week 16, compared to the former. However, the plate with a 4.7 mm thickness performs remarkably better in providing the necessary mechanical stimulus at the fracture site, as it results in 8.88% more differentiation of granulation tissue through fibro-cartilaginous pathway of healing, compared to that of 8 mm thick LCP, at the end of first week after surgery. Thus, if the maturity of hard callus, and the propensity of initial tissue to differentiates via secondary pathway of healing, were assumed to have the same

order of importance in the secondary healing process of a fractured bone, it is obvious that an LCP with a thickness equals to 4.7 mm is superior to the LCPs with a thickness of 8 mm. Recently, Sheng and co-workers used experimentally validated FE models, without modeling tissue differentiation at the fracture gap, and found the optimal thickness of 4.6 mm for the internal fixation of femoral mid-shaft fracture, fixed by an 10-holes LCP, using a comprehensive optimization process for the LCP system.[44]

It should be noted that, monitoring of differentiation pattern was limited to just axial compressive load in this work. The main reason for this simplification was that all theories that have been developed in regard to mechanobiology of bone healing are solely concerned with the axial compressive load, as the predominant force at the fracture site of a long bone.[11,16,18] Nonetheless, it is known that when an implanted bone is subjected to a variety of rehabilitation practices after surgery, a combination of various modes of loads can be observed at the fracture site. Further development in mechanobiology of bone healing would be of great help in gaining a deeper insight into the underlying healing mechanism, and also in establishing more efficient implants for superimposed load configurations. Moreover, based on the phenomenological computational model used in this study, deviatoric strain explains progressive tissue regeneration within the callus. A more comprehensive mechanobiological model, which could take into account not only mechanical stimuli for tissue differentiation, but also encompasses mechanical modulation of cellular activities, matrix synthesis, callus growth, vascular network regeneration and growth factors in bone healing process, could surely offers more accurate results, compared to the outcomes of this study. Another simplification made in this study was to model tibia as a long cylinder with a constant modulus of elasticity, as well as constant inner and outer diameters. Also, threads of screws and curves of the cross sectional profile of real LCPs were disregarded here. To improve the accuracy of this procedure, more realistic material and structural properties should be assigned to each component of the bone-plate construct in future studies. Additionally, material and structural properties of the bone-LCP-screw construct, as well as loading condition applied to the model can most likely alter the optimal thickness of the LCP. Thus, in order to determine an optimal LCP thickness for a bone-LCP construct with specifications different from those assumed in this study, further analyses should be made, but through employing the same approach suggested here.

Conclusion

Instead of concentrating on a single aspect of a long bone fixation and fracture healing process, in this study a computational-based multi-objective approach was

employed, which different criteria including secondary healing process, strength and stability of the bone-plate construct were taken into account. The results of this study showed that, through employing the aforementioned design criteria, a thickness of 4.7 mm can provide a superior fixation with an optimal performance. This work can be deemed as a step toward a mechanobiologically designed bone plate paradigm, with the aim of finding an optimal bone-plate construct by compromising between the bone-plate strength/stability, and the bone secondary healing process quality.

ORCID iDs

Yousof Mohandes [ID] https://orcid.org/0000-0002-6528-9090

Gholamreza Rouhi [ID] https://orcid.org/0000-0001-5592-4970

References

1. Idkaidek A and Jasiuk I. Cortical bone fracture analysis using XFEM–case study. *Int J Numer Meth Bio* 2017; 33(4): e2809.
2. Zimmermann EA, Gludovatz B, Schaible E, et al. Fracture resistance of human cortical bone across multiple length-scales at physiological strain rates. *Biomaterials* 2014; 35: 5472–5481.
3. Zioupos P, Currey JD and Casinos A. Tensile fatigue in bone: are cycles-, or time to failure, or both, important? *J Theor Biol* 2001; 210: 389–399.
4. Giannoudis P and Schneider E. Principles of fixation of osteoporotic fractures. *Bone Joint J* 2006; 88: 1272–1278.
5. Wei S, Wang S, Wang DM, et al. Biomechanical analysis of femoral fixation with a new compression plate using finite element method during stair climbing. *Key Eng Mater* 2016; 693: 297–305.
6. Perren SM. Evolution of the internal fixation of long bone fractures: the scientific basis of biological internal fixation: choosing a new balance between stability and biology. *Bone Joint J* 2002; 84: 1093–1110.
7. Gervais B, Vadean A, Raison M, et al. Failure analysis of a 316L stainless steel femoral orthopedic implant. *Case Stud Eng Fail Anal* 2016; 5: 30–38.

8. Gardner MJ, Evans JM and Dunbar RP. Failure of fracture plate fixation. *J Am Acad Orthop Surg* 2009; 17: 647–657.
9. Samiezadeh S, Avval PT, Fawaz Z, et al. On optimization of a composite bone plate using the selective stress shielding approach. *J Mech Behav Biomed* 2015; 42: 138–153.
10. Doblaré M, Garcıa J and Gómez M. Modelling bone tissue fracture and healing: a review. *Eng Fract Mech* 2004; 71: 1809–1840.
11. Carter DR, Beaupré GS, Giori NJ, et al. Mechanobiology of skeletal regeneration. *Clin Orthop Relat R* 1998; 355: S41–S55.
12. Kenwright J and Goodship AE. Controlled mechanical stimulation in the treatment of tibial fractures. *Clin Orthop Relat R* 1989; 241: 36–47.
13. Pauwels F, Maquet PG and Furlong R. *Biomechanics of the locomotor apparatus: contributions on the functional anatomy of the locomotor apparatus.* Berlin Heidelberg: Springer, 2012.
14. Cheal E, Mansmann K, Digioia AM, et al. Role of interfragmentary strain in fracture healing: ovine model of a healing osteotomy. *J Orthop Res* 1991; 9: 131–142.
15. Carter D, Blenman P and Beaupre G. Correlations between mechanical stress history and tissue differentiation in initial fracture healing. *J Orthop Res* 1988; 6: 736–748.
16. Prendergast P, Huiskes R and Søballe K. Biophysical stimuli on cells during tissue differentiation at implant interfaces. *J Biomech* 1997; 30: 539–548.
17. Claes LE, Heigele CA, Neidlinger-Wilke C, et al. Effects of mechanical factors on the fracture healing process. *Clin Orthop Relat R* 1998; 355: S132–S147.
18. Isaksson H, Wilson W, van Donkelaar CC, et al. Comparison of biophysical stimuli for mechano-regulation of tissue differentiation during fracture healing. *J Biomech* 2006; 39: 1507–1516.
19. Haase K and Rouhi G. A discussion on plating factors that affect stress shielding using finite element analysis. *J Biomech Eng T Asme* 2010; 5: 129–141.
20. Bagheri ZS, Avval PT, Bougherara H, et al. Biomechanical analysis of a new carbon fiber/flax/epoxy bone fracture plate shows less stress shielding compared to a standard clinical metal plate. *J Biomech Eng* 2014; 136: 091002.
21. Chaya A, Yoshizawa S, Verdelis K, et al. In vivo study of magnesium plate and screw degradation and bone fracture healing. *Acta Biomater* 2015; 18: 262–269.
22. Ganesh V, Ramakrishna K and Ghista DN. Biomechanics of bone-fracture fixation by stiffness-graded plates in comparison with stainless-steel plates. *Biomed Eng Online* 2005; 4: 46.
23. Fouad H. Effects of the bone-plate material and the presence of a gap between the fractured bone and plate on the predicted stresses at the fractured bone. *Med Eng Phys* 2010; 32: 783–789.
24. Andreykiv A, Van Keulen F and Prendergast P. Simulation of fracture healing incorporating mechanoregulation of tissue differentiation and dispersal/proliferation of cells. *Biomech Model Mechan* 2008; 7: 443–461.
25. Huiskes R, Janssen J and Slooff T. A detailed comparison of experimental and theoretical stress-analyses of a human femur. *Mech Prop Bone* 1981; 45: 211–234.

26. Mehboob H and Chang S-H. Application of composites to orthopedic prostheses for effective bone healing: a review. *Compos Struct* 2014; 118: 328–341.

27. Miramini S, Zhang L, Richardson M, et al. Influence of fracture geometry on bone healing under locking plate fixations: a comparison between oblique and transverse tibial fractures. *Med Eng Phys* 2016; 38: 1100–1108.

28. Ahmad M, Nanda R, Bajwa A, et al. Biomechanical testing of the locking compression plate: when does the distance between bone and implant significantly reduce construct stability? *Injury* 2007; 38: 358–364.

29. Xue Z, Xu H, Ding H, et al. Comparison of the effect on bone healing process of different implants used in minimally invasive plate osteosynthesis: limited contact dynamic compression plate versus locking compression plate. *Sci Rep* 2016; 6: 37902.

30. Buckley RE, Moran CG and Apivatthakakul T. *AO principles of fracture management: Vol. 1: principles, Vol. 2: specific fractures.* Thieme Medical Publishers, Incorporated, 2017.

31. Grant C. *Mechanical testing and modelling of a bone-implant construct.* PhD thesis, Queensland University of Technology, 2012.

32. Lacroix D and Prendergast P. Three-dimensional simulation of fracture repair in the human tibia. *Comput Method Biomec* 2002; 5: 369–376.

33. Wolfram U and Schwiedrzik J. Post-yield and failure properties of cortical bone. *BoneKEy Rep* 2016; 5.

34. ASTM F138-13, Standard Specification for Wrought 18 Chromium-14 Nickel-2.5 Molybdenum Stainless Steel Bar and Wire for Surgical Implants (UNS S31673), ASTM International, West Conshohocken, PA, 2013, www.astm.org.

35. Karakasli A, Basci O, Ertem F, et al. Dual plating for fixation of humeral shaft fractures: A mechanical comparison of various combinations of plate lengths. *Acta Orthop Traumatol Turc* 2016; 50: 432–436.

36. Nourisa J and Rouhi G. Biomechanical evaluation of intramedullary nail and bone plate for the fixation of distal metaphyseal fractures. *J Mech Behav Biomed* 2016; 56: 34–44.

37. Augat P, Burger J, Schorlemmer S, et al. Shear movement at the fracture site delays healing in a diaphyseal fracture model. *J Orthop Res* 2003; 21: 1011–1017.

38. Lacroix D and Prendergast P. A mechano-regulation model for tissue differentiation during fracture healing: analysis of gap size and loading. *J Biomech* 2002; 35: 1163–1171.

39. Isaksson H, Van Donkelaar CC, Huiskes R, et al. Corroboration of mechanoregulatory algorithms for tissue differentiation during fracture healing: comparison with in vivo results. *J Orthop Res* 2006; 24: 898–907.

40. Bottlang M, Doornink J, Lujan TJ, et al. Effects of construct stiffness on healing of fractures stabilized with locking plates. *J Bone Joint Surg Am* 2010; 92: 12.

41. Gómez-Benito M, García-Aznar J, Kuiper J, et al. A 3D computational simulation of fracture callus formation: influence of the stiffness of the external fixator. *J Biomech Eng* 2006; 128: 290–299.

42. Wu J-J, Shyr H, Chao E, et al. Comparison of osteotomy healing under external fixation devices with different stiffness characteristics. *J Bone Joint Surg Am* 1984; 66: 1258–1264.

43. Arora JS. *Introduction to optimum design.* San Diego, California: Elsevier, 2004.

44. Sheng W, Ji A, Fang R, et al. Finite element-and design of experiment-derived optimization of screw configurations and a locking plate for internal fixation system. *Comput Math Methods Med* 2019; 2019: 5636528.